Scattering differentiates Alzheimer disease *in vitro*

Eugene B. Hanlon,[1,*] Lev T. Perelman,[2] Eduard I. Vitkin,[2] Frank A. Greco,[1] Ann C. McKee,[1,3] and Neil W. Kowall[1,3]

[1]*Department of Veterans Affairs, Office of Research and Development, and Geriatric Research, Education and Clinical Center, 200 Springs Road, Bedford, Massachusetts 01730, USA*

[2]*Department of Obstetrics, Gynecology and Reproductive Biology, Harvard Medical School and Beth Israel Deaconess Medical Center, 30 Brookline Avenue, Boston, Massachusetts 02215, USA*

[3]*Departments of Neurology and Pathology and Laboratory Medicine, Boston University School of Medicine, 715 Albany Street, Boston, Massachusetts 02118, USA*

**Corresponding author: Eugene.Hanlon@med.va.gov*

Received November 20, 2007; revised February 6, 2008; accepted February 8, 2008; posted February 12, 2008 (Doc. ID 89838); published March 14, 2008

The molecular bases of Alzheimer disease and related neurodegenerative disorders are becoming better understood, but the means for definitive diagnosis and monitoring *in vivo* remain lacking. Near-infrared optical spectroscopy offers a potential solution. We acquired transmission and reflectance spectra of thin brain tissue slabs, from which we calculated wavelength-dependent absorption and reduced scattering coefficients from 470–1000 nm. The reduced scattering coefficients in the near infrared clearly differentiated Alzheimer from control specimens. Diffuse reflectance spectra of gross brain tissue *in vitro* confirmed this observation. These results suggest a means for diagnosing and monitoring Alzheimer disease *in vivo*, using near-infrared optical spectroscopy. © 2008 Optical Society of America

OCIS codes: 170.0170, 170.3660, 170.6510, 290.5825.

Alzheimer disease (AD), the most common form of dementia seen in clinical practice, is a progressive, terminal, neurodegenerative disorder. The largest risk factor for AD is advanced age, and the public health impact of AD and related disorders is increasing in proportion to the increasing numbers of elderly. AD presents clinically as progressive memory loss, but the only definitive diagnostic tests that now exist require neuropathologic examination of brain tissue, conducted almost exclusively postmortem.

As knowledge of the molecular features of AD and related neurodegenerative disorders advances, strategies for pharmaceutical interventions that implement this knowledge are being vigorously pursued [1]. However, to our knowledge there is currently no method for monitoring pathogenic response to such interventions in human clinical trials or for definitively diagnosing these disorders at an early stage, where intervention could be most beneficial.

Numerous articles document efforts to apply conventional medical imaging techniques to the diagnosis and monitoring of AD [2]. Magnetic resonance imaging (MRI) has provided a wealth of functional [3] or anatomic [4] information. Development of radionuclide markers targeting parenchymal amyloid deposits is a breakthrough in the application of positron emission tomography (PET) [5]. Even optical techniques, while not yet widely applied in clinical practice as MRI or PET, have made parallel contributions to these efforts, utilizing functional information [6,7] or exogenous markers in mice [8].

We prepared spectroscopy samples from unstained, unfixed, postmortem temporal poles, flash frozen at autopsy and brought to room temperature immediately before measurement, thus minimizing postmortem and freeze-thaw effects. All brains were neuropathologically confirmed as AD or non-AD control.

We prepared thin tissue slabs for transmission and reflectance measurements from each of two AD and two non-AD brains. Each AD case was late stage, Braak stage V and Braak stage VI [9]. Specimens were partially thawed to obtain microtomed sections approximately 1 mm thick. Fully thawed tissue samples were mounted in optical cells with 1 mm path length and .15 mm thick windows. The tissue fully contacted the cell windows but was not compressed in the cell. Cells were mounted in the integrating sphere of a Cary 5 spectrometer. For reflectance measurements, the geometry to reject specular reflection of the incident beam was used. Total integrated reflectance and transmission spectra were acquired over the wavelength range 470–1000 nm. Elapsed time from tissue sectioning to completion of data acquisition was less than 4 hours.

For gross tissue diffuse reflectance measurements, one temporal pole from each of five AD and four non-AD brains was used. Each temporal pole was several cubic centimeters in volume. Each specimen was placed on a microscope cover slip that fully supported it. Incident light from a water-filtered Xe arc source, coupled into the central fiber optic of a low –OH fiber bundle, was delivered to the air-exposed surface of the tissue from a distance of 10 mm, providing a spot size of 15 mm^2. The incident angle was 30°, to minimize the specular component of the detected reflectance signal. The cover slip was mounted to provide a free path to a mirror positioned about 20 cm below, which had been oriented to divert light that had propagated through the sample and cover slip from possible backreflection into the signal detection fibers. Six detection fibers were arranged around the delivery fiber concentrically, in a close-packed arrangement; all fibers were 200 μm core, NA=0.22. The proximal termination of the detection fibers was

 © 2008 Optical Society of America

a linear array that was positioned at the 100 μm entrance slit of an Acton Spectra-Pro 150 spectrograph coupled to an Andor DU 434 FI CCD, TE cooled to −60 °C.

Figure 1 shows a set of transmission (T) and reflectance (R) spectra for 1 mm thick tissue slabs of one AD specimen and one non-AD control specimen. To describe light propagation in the brain tissue slabs, we adapted the two flux model implicitly derived from the radiative transport equation [10]. The resulting equations, used to describe the tissue reflectance, R, and transmission, T, in terms of the absorption coefficient (μ_a) and reduced scattering coefficient (μ_s') are presented in Eqs. (1) and (2):

$$R = \frac{1 - r^2}{r} C, \tag{1}$$

$$T = \left[C - \frac{r\Lambda}{2(1-r)(1+\gamma)} (1 - \exp[-1(1+\lambda)\tau]) \right] \exp(\gamma\tau) + \left[-C + \frac{\Lambda}{2(1-r)(1+\gamma)} (1 - \exp[-1(1-\lambda)\tau]) \right] \times \exp(-\gamma\tau), \tag{2}$$

where

$$C = r\Lambda/2(1-r)(1+\gamma)(1 - r^2 \exp(-2\gamma\tau)) \times \left[1 - r((1+\gamma)/(1-\gamma)) \exp(-2\gamma\tau) + \left(r((1+\gamma)/(1-\gamma)) - 1\right)\exp(-(1+\gamma)\tau)\right]$$

$$r = [(a(1-\Lambda) - \gamma/b\Lambda] - 1,$$

$\gamma = a[(1-\Lambda)(1-\Lambda+2b/a\Lambda)]^{1/2}$, $\Lambda = \mu_s'/(\mu_a + \mu_s')$, and $\tau = (\mu_a + \mu_s')L$, where L is the tissue thickness.

To apply this model to the observed reflectance and transmission spectra requires evaluation of the parameters a and b, which include the effects of the phase function and boundary conditions. We determined these two parameters by fitting the reflectance and transmission modeled by Eqs. (1) and (2) to Monte Carlo simulations. Figure 2 shows the fit of modeled reflectance and transmission to Monte Carlo simulations for $a = 1.859$ and $b = 0.5536$, for biomedically relevant values for μ_a and μ_s'; for reflectance, the largest error is less than 3%. Using these values for a and b, we determined the values of μ_a and μ_s' that gave the best fit of the model to the observed reflectance and transmission spectra. Figure 3 presents the wavelength-dependent optical constants for AD and normal brain tissues over the wavelength range 470–1000 nm, which are consistent with prior reports at single or a few wavelengths [11,12].

Scattering shows a clear difference between AD and non-AD tissue, while absorption, dominated by hemoglobin, provides less distinction. Importantly, the slope of the wavelength-dependent reduced scattering coefficient for AD brain is distinct from that of non-AD control.

Figure 4 shows mean diffuse reflectance spectra of the intact temporal pole specimens from AD and non-AD control cases. Each mean spectrum is the average of five AD and four non-AD spectra (one spectrum per specimen) for each diagnosis. The diffuse reflectance spectra confirm that scattering and slope, particularly in the range of 670–970 nm, where there is little absorption, significantly differentiate AD brain tissue from non-AD control brain tissue, with $p = 0.005$ for slope and $p = 0.002$ for intensity (two-tailed, Student's t-test).

The definitive neuropathologic features that distinguish AD from normal brain are neuritic plaques (NPs) and neurofibrillary tangles (NFTs). NPs are predominantly extracellular deposits of β-amyloid peptide fibrils, and NFTs are intraneuronal accumulations of abnormally phosphorylated and oxidized tau protein.

The increased scattering observed for AD brain tissue compared with control brain tissue is consistent

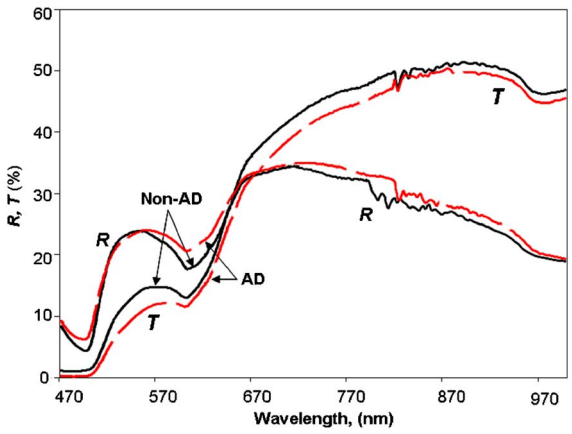

Fig. 1. (Color online) Total reflectance (R) and transmission (T) spectra, acquired with an integrating sphere, of 1 mm thick brain tissue slabs from confirmed AD (broken curve) and non-AD (solid curve) cases.

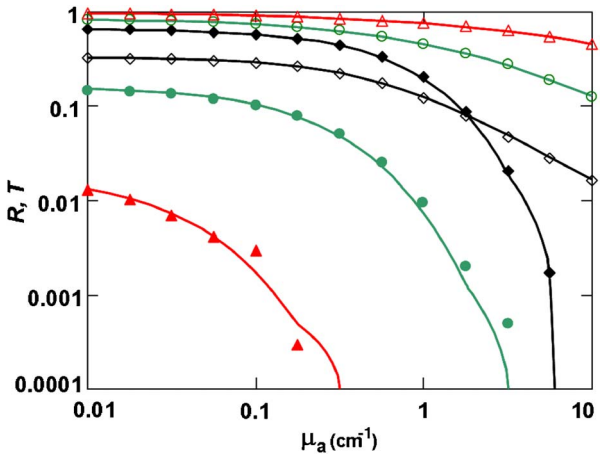

Fig. 2. (Color online) Reflectance and transmission (R, T) calculated for a turbid slab of 1 mm thickness using Eqs. (1) and (2) (solid curve) and Monte Carlo simulations (symbols) over a range of $0.01 \le \mu_a \le 10.0$ (cm^{-1}) and $1 \le \mu_s' \le 100$ (cm^{-1}). Open symbols indicate reflectance; solid symbols indicate transmission. Triangles, $\mu_s' = 100$ cm^{-1}; circles, $\mu_s' = 10$ cm^{-1}; diamonds, $\mu_s' = 1$ cm^{-1}.

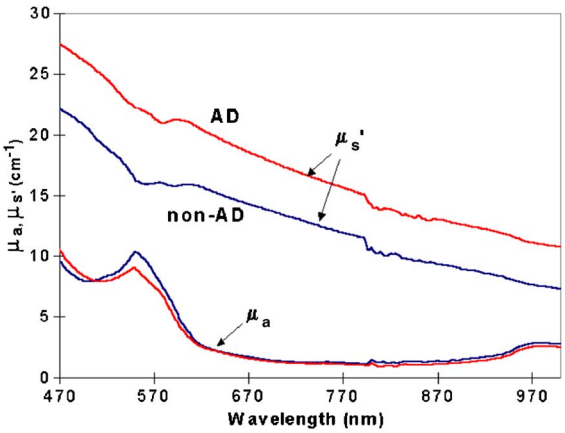

Fig. 3. (Color online) Absorption (μ_a) and reduced scattering (μ_s') coefficients for non-AD and AD brain tissue obtained by fitting Eqs. (1) and (2) to experiment (Fig. 1).

with the histopathologic changes known to occur in AD, in the form of NPs and NFTs. Both NPs and NFTs are dense protein aggregates whose characteristic physical chemical properties are distinct from surrounding tissue. As such, NPs and NFTs should behave as small light-scattering particles that contribute to the reported differences between diseased and nondiseased brain tissue: the presence of NP and NFT increase light scattering in the AD brain. Furthermore, the characteristic sizes of NPs and NFTs, several tens of micrometers, would be expected to contribute to a steeper slope in the long-wavelength region of the scattering spectrum, because they are large scatterers compared with the surrounding light-scattering tissue compartments (nuclei, organelles, etc.) [13]. This again is consistent with the steeper slope observed for AD compared with non-AD brain tissue in the 670–970 nm region of the reported spectra.

Near-infrared (NIR) light propagates harmlessly through the overlying tissue, bone, and cerebrospinal

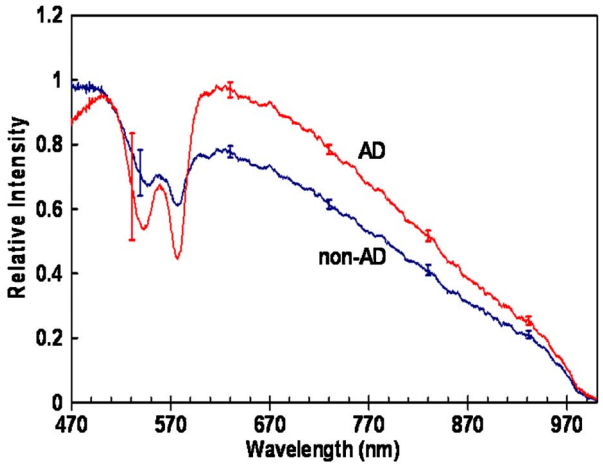

Fig. 4. (Color online) Mean diffuse reflectance spectra of intact temporal pole specimens from neuropathologically confirmed AD cases (AD), $n=5$, and control cases (non-AD), $n=4$. Error bars indicate the standard error of the mean for the AD and non-AD populations based on the spectra measured for each group.

fluid to probe the brain noninvasively. Histopathological features of AD such as NPs and NFTs are dense protein aggregates distinct from normal histology, which should provide characteristic light-scattering signatures. These and other features of AD pathology may also contribute distinct NIR fluorescence [14] and absorption spectra as well. Thus a direct connection between the inherent optical properties of brain tissue and the known neuropathological features of AD and related neurodegenerative diseases can be provided by NIR optical spectroscopy, without the need for exogenous markers.

This work was supported by the U.S. Department of Veterans Affairs, Office of Research and Development, Medical Research Service and by National Science Foundation (NSF) grant BES-0116833 and CIMIT New Concept Award. The Boston University Alzheimer's Disease Research Center (NIH AG-13846) provided tissue specimens and neuropathology, and the NSF-supported Center for Materials Science and Engineering at MIT provided the Cary spectrometer and technical assistance.

References

1. M. C. Irizarry and B. T. Hyman, J. Neuropathol. Exp. Neurol. **60**, 923 (2001).
2. A. Coimbra, D. S. Williams, and E. D. Hostetler, Curr. Top Med. Chem. **6**, 629 (2006).
3. M. M. Machulda, H. A. Ward, B. Borowski, J. L. Gunter, R. H. Cha, P. C. O'Brien, R. C. Petersen, B. F. Boeve, D. Knopman, D. F. Tang-Wai, R. J. Ivnik, G. E. Smith, E. G. Tangalos, and C. R. Jack, Neurology **61**, 500 (2003).
4. C. R. Jack, M. M. Shiung, S. D. Weigand, P. C. O'Brien, J. L. Gunter, B. F. Boeve, D. S. Knopman, G. E. Smith, R. J. Ivnik, E. G. Tangalos, and R. C. Petersen, Neurology **65**, 27 (2005).
5. C. A. Mathis, Y. Wang, and W. E. Klunk, Curr. Pharm. Des. **10**, 1469 (2004).
6. C. Hock, K. Villringer, F. Muller-Spahn, R. Wenzel, H. Heekeren, S. Schuh-Hofer, M. Hofmann, S. Minoshima, M. Schwaiger, U. Dirnagl, and A. Villringer, Brain Res. **755**, 293 (1997).
7. G. Strangman, J. P. Culver, J. H. Thompson, and D. A. Boas, Neuroimage **17**, 719 (2002).
8. M. Hintersteiner, A. Enz, P. Frey, A. Jaton, W. Kinzy, R. Kneuer, U. Neumann, M. Rudin, M. Staufenbiel, M. Stoeckli, K. Wiederhold, and H. Gremlich, Nat. Biotechnol. **23**, 577 (2005).
9. H. Braak and E. Braak, Acta Neuropathol. (Berl) **82**, 239 (2005).
10. E. P. Zede, A. P. Ivanov, and I. L. Katsev, *Image Transfer Through a Scattering Medium* (Springer-Verlag, 1991).
11. P. Van der Zee, M. Essenpreis, and D. T. Delpy, Proc. SPIE **1888**, 454 (1993).
12. W. F. Cheong, S. A. Prahl, and A. J. Welch, IEEE J. Quantum Electron. **26**, 2166 (1990).
13. L. T. Perelman, V. Backman, M. Wallace, G. Zonios, R. Manoharan, A. Nusrat, S. Shields, M. Seiler, C. Lima, T. Hamano, I. Itzkan, J. Van Dam, J. M. Crawford, and M. S. Feld, Phys. Rev. Lett. **80**, 627 (1998).
14. E. B. Hanlon, I. Itzkan, R. R. Dasari, M. S. Feld, R. J. Ferrante, A. C. McKee, D. Lathi, and N. W. Kowall, Photochem. Photobiol. **70**, 236 (1999).